Biodegradable doubly cross-linked chitosan hydrogels as sustained drug delivery systems. Influence of chemical cross-linking and chitosan ratios on rheological properties and pharmacological performance.

Nieves Iglesias[1], Elsa Galbis[1], Concepción Valencia[2,3], M. Jesús Díaz-Blanco[2,3], Bertrand Lacroix[4,5], M.-Violante de-Paz[1,]*

1. Departamento de Química Orgánica y Farmacéutica, Facultad de Farmacia, Universidad de Sevilla, 41012 Sevilla, Spain
2. Departamento de Ingeniería Química, Campus de "El Carmen", Universidad de Huelva, 21071 Huelva, Spain
3. Pro2TecS—Chemical Process and Product Technology Research Center, Universidad de Huelva, 21071 Huelva, Spain
4. Department of Materials Science and Metallurgical Engineering, and Inorganic Chemistry, University of Cádiz, Cádiz, Spain.
5. IMEYMAT, Institute of Research on Electron Microscopy and Materials of the University of Cádiz, Cádiz, Spain.

*Correspondence: vdepaz@us.es; Tel.: +34-954-556-740

Abstract

This study investigates the impact of dual ionic and covalent cross-links (ion-XrL and cov-XrL) on the properties of chitosan-based (CTS) hydrogels as eco-friendly drug delivery systems (DDS) for the model drug diclofenac sodium (DCNa). Citric acid and a diiodo-trehalose derivative (ITrh) were the chosen ionic and covalent cross-linker, respectively. The novel hydrogels completely disintegrated within 96 h by means of a hydrolysis process mediated by the enzyme trehalase. As far as the authors are aware, this is the first time that a trehalose derivative has been used as a covalent cross-linker in the formation of biodegradable hydrogels. The impact of CTS concentration and degree of cov-XrL on rheological parameters were examined by means of an experimental model design and marked differences were found between the materials. Hydrogels with maximum elastic properties were achieved at high CTS concentrations and high degrees of cov-XrL. DCNa-loaded formulations displayed well-controlled drug-release profiles strongly dependent on formulation composition (from 17% to 40% in 72 h). Surprisingly, higher degrees of covalent cross-linking led to a boost in drug release. The formulations presented herein provides a simple and straightforward pathway to design fully biodegradable, tailor-made controlled drug delivery systems with improved rheological properties.

Keywords:

Ionic cross-linking; chemical cross-linking; controlled drug release; biodegradable; eco-friendly formulations; viscoelastic hydrogels.

1. Introduction

Hydrogels constitute a group of polymeric materials that swell and retain a significant fraction of water within their three-dimensional (3D). They exhibit tunable mechanical properties, biocompatibility and biodegradability and are therefore widely applied in biomedical and pharmaceutical fields: cell proliferation and differentiation [1], tissue engineering and regenerative medicines [2,3], and wound dressing [4,5], among others. However, one of their most promising uses is as a constituent of matrices for the controlled release of bioactive molecules, [6,7]. For hydrogel applications as drug delivery systems (DDS), their original 3D structure must be mechanically strong so that they do not erode prematurely, and thus early release or diffusion of the drug to non-target tissues is prevented. This would dramatically improve their therapeutic efficacy and reduce drug-associated side effects [8]. Moreover, it is necessary their disintegration under physiological conditions, preferably in harmless products to ensure a good biocompatibility of the hydrogel [9].

Although hydrogels made from natural polymers may not provide sufficient mechanical properties, they do offer their inherent biocompatibility as an advantageous property [10]. Therefore, strengthen the natural-based hydrogel system while maintaining its swelling, flexibility and degradability properties is pursued. Among the natural occurring polymers, chitosan (CTS) is drawing the attention of the scientific community, in particular, in biomedical applications because of its interesting biopharmaceutical characteristics, well documented biocompatibility and low toxicity [11]. CTS is also able to adhere to the mucosal surfaces within the body [8] and has demonstrated its capacity to open tight junctions between epithelial cells though well-organized epithelia [12] acting as a permeation enhancer.

An interesting review provides an overview of traditionally used and recently developed methods for preparation and modification of chitosan-based hydrogels [13]. In general, crosslinkers serve as a bridge linking different or the same polymer chains, forming a 3D network, improving the mechanical strength and chemical stability in acidic solutions. CTS hydrogels have been prepared via ionotropic gelation (ionic cross-linking) [2,14–18]

coordination with metal ions [19], and irreversible/covalent cross-linking between CTS and the cross-linker [7,20–22], among others. Among the covalent stabilization mechanism, one of the most widely used is the formation of imine bonds between amino groups from CTS and the aldehyde groups from the cross-linker [8,23,24].

Although non-covalent cross-linked hydrogels show unique mechanical properties, including both stiffness/toughness and elasticity/flexibility to retain the hydrogel structure, most of them are mechanically weak and prone to fracture, greatly restricting their applications [25]. Conversely, and regarding drug release, the reversible nature of ionically cross-linked networks is useful since, once release in the drug in the medium has been achieved, the formulations can subsequently disintegrate into biocompatible components that then will be metabolized and eliminated from the body [26].

Different approaches can be followed to overcome the instability of ionotropic hydrogels. Thus, for example; to improve the mechanical properties of ionically cross-linked calcium-alginate hydrogels under physiological conditions, the formation of interpenetrating polymer network was successfully conducted by Zhao *et al.* [27]. On the other hand, covalent cross-linking can improve the mechanical properties of the hydrogels [28] and consequently, dual covalent and ionic bonds can be considered as an effective method to enhance the properties of CTS-based materials. However, only few examples of dual cross-linking methods have been published. Zhuang *et al.* reported the formation of CTS films through the utilization of citric acid as a dual ionic and covalent linker [29]. Ionic and covalent cross-linking of CTS with $CaSO_4$ and genipin, respectively, has also been investigated [30]. Additionally, cross-linked iminoboronate-CTS hydrogels have also been reported in which boronate-based coordination and covalent cross-linking occur [31]. On the other hand, when chemical cross-linking is involved, a decrease in degradability is usually observed [28]. Labile bonds need being introduced in the gels so that the former can be broken under physiological conditions. Thus, ensuring the presence of labile covalent bonds in the chemical structure of the covalent cross-linkers is a good strategy to overcome this drawback. Among the breakable covalent bonds, glycosidic linkages are present in di-, oligo- or polysaccharides. They are easily hydrolyzed by living systems by means of reactions catalyzed by extremely

common non-specific and specific glycosidase enzymes {also called glycoside hydrolases, [32,33]}, such as cellulase, amylase, mannosidase, lactase and trehalase, among others.

In this work, we aim to manufacture a set of biodegradable and eco-friendly chitosan-based hydrogels with enhanced rheological properties as DDS by means of a double cross-linking process. Sodium diclofenac (DCNa), one of the most frequently used non-steroidal anti-inflammatory drugs (NSAID) was the model drug of choice. The hydrogels were ionically and covalently cross-linked. The chosen covalent cross-linker was the 2,3,4,2',3',4'-hexa-*O*-acetyl-6,6'-diiodo-6,6'-dideoxy-α-D-Glucopyranosyl-α-D-glucopyranoside (ITrh), a dielectrophilic derivative from the disaccharide α,α'-trehalose, that bears a labile acetal group in its structure. As ionic cross-linker, citric acid (CA) was the polyprotic acid of choice since it presents excellent antimicrobial and antioxidant properties as well as excellent biocompatibility [29,34]. The chemical structure, biodegradability under physiological conditions, thermogravimetric properties and morphologies of the hydrogels were evaluated. Two parameters, CTS concentration and degree of covalent cross-linking, were investigated to find the influence they exerted not only on the physicochemical and rheological properties of the hydrogels prepared based on CTS, but also on the release profiles of DCNa. Drug release tests under physiological conditions were conducted to demonstrate the in vitro controlled drug release of DCNa. The prepared CTS-based hydrogels have demonstrated to be fully biodegradable and endowed with controlled DCNa release properties under physiological conditions for advanced therapies in which dual ionic and covalent cross-links were involved. As far as the authors are aware, this is the first time that a trehalose derivative has been used as a biodegradable covalent cross-linker in the formation of structured polymeric materials.

2. Materials and methods

2.1. Materials

All the chemicals used were purchased from Sigma-Aldrich (Madrid, Spain) and used as received. The phosphate buffer solution of pH 5.5 (25 °C) used for release assays was

freshly prepared when required. Chitosan (CTS) from Sigma-Aldrich, with a deacetylation degree of 75% was chosen. The molecular weight of the CTS was determined by viscometric analysis. Its viscosity was measured in a buffered solution of 0.5 M acetic acid - 0.5 M sodium acetate solution at 25.0 ± 0.1 °C using an Anton Paar AMVn automated microviscometer. The viscometric constants "a" and "K" in the Mark-Houwink equation were previously determined for this solvent — CTS system and found to be a = 0.59 and K = 0.119 $cm^3\ g^{-1}$. The weight of the CTS used was calculated by means of the Mark-Houwink equation ([η] = 3.385 dL/g) and its value was 299 kDa. The di-iodinated trehalose (ITrh) employed for covalent crosslinking (cov-XrL) was prepared following the recipe described in Section 2.2.2. Trehalase (from porcine kidney, 1UN/0.5 mL) was supplied by Sigma–Aldrich, Spain.

Dialysis tubing cellulose membranes avg. flat width 25 mm (Mw 8,000-14,000) were purchased from Sigma-Aldrich. Before the release, it was necessary to activate the cellulose membrane of the dialysis tube following this procedure: washing the tubing in water for 3 h, treating the tubing with a 0.3% (w/v) solution of sodium sulfide at 80 °C for 1 min. Subsequently it was washed with water at 60 °C for 2 min and with a 0.2% (v/v) solution of sulfuric acid. Finally, it was washed with hot water the acid.

2.2. Methods

2.2.1. General Methods

Fourier Transform Infrared (FTIR) spectra were recorded on a Jasco FT/IR 4200 spectrometer (Great Dunmow, Essex, UK) equipped with attenuated total single reflection (ATR) accessory in the wavenumber range from 4000 to 400 cm^{-1}. Nuclear magnetic resonance (NMR) and mass spectra were recorded at the CITIUS Service (University of Seville). ^1H and ^{13}C NMR spectra were recorded at 300 K with a Bruker AMX-500 for solutions in $CDCl_3$. Chemical shifts (δ) are reported as parts per million downfield from Me_4Si and J in Hz. J is assigned and not repeated. All the assignments were confirmed by COSY and HSQC experiments. Mass spectra were obtained using a Kratos MS80RFA instrument. High resolution mass spectra were recorded on a Q-Exactive spectrometer.

2.2.2. Synthesis of 2,3,4,2',3',4'-Hexa-*O*-acetyl-6,6'-diiodo-6,6'-dideoxy-α-D-Glucopyranosyl-α-D-glucopyranoside (ITrh)

The title compound was prepared according to a modified method of the procedure followed by Sizovs *et al.* [35]. A suspension of iodine (22.23 g, 87.6 mmol) in dry dimethylformamide (DMF, 200 mL) was prepared in round-bottom flask. A solution of triphenylphosphine (24.20 g, 92.27 mmol) in dry tetrahydrofuran (THF, 38 mL) was added to the iodine suspension followed by anhydrous trehalose (10 g, 29.2 mmol). The reaction was allowed to proceed at 80 °C for 12 h and the solvents were removed under reduced pressure. The resulting syrup was dissolved in methanol (250 mL) and basified to pH 9 by means of sodium methoxide. The mixture was stirred for 2 h at r.t. and then neutralized by the addition of the acidic resin DOWEX-2H (H^+ form). Methanol was removed under reduced pressure to yield a colored oil that was poured into water (150 mL). To facilize the precipitation of the formed triphenylphosphine oxide, the aqueous solution was stored at 4 °C for 24 h. A white solid appeared at the bottom of the flask and the suspension was then filtered and washed with dichloromethane (DCM, 2 x 50 mL). The water from the aqueous solution was mostly removed under reduced pressure, and the obtained oil was dried at high vacuum for 48 h in the presence of P_2O_5. The dry oil was dissolved in dry pyridine (Py, 200 mL) and the solution was placed in an ice-bath. Acetic anhydride (38 mL, 403 mmol) was slowly added and the reaction was allowed to stir at 25 °C for 12 h. The reaction mixture was poured on ice, and then extracted with dichloromethane (DCM, 4 x 50 mL). The combined organic layers were washed with a dilute solution of sulfuric acid and dried over Na_2SO_4. Na_2SO_4 was filtered off and the solvent removed under reduced pressure yielding a yellowish oil. The product was purified by column chromatography (eluent gradient: from 1:1 *tert*-butyl methyl ether-hexane to 1:4 *tert*-butyl methyl ether-hexane) to yield the title compound (23.2 g, 25.0%). The ITrh spectra are recorded in Figures S1 to S4 in Supplementary information.

^{1}H-NMR (500 MHz, $CDCl_3$) δ ppm: 5.55 – 5.46 (m, 2H, H-3), 5.42 (d, 2H, H-1, $J_{1,2}$ = 4.0 Hz), 5.19 (dd, 2H, H-2, $J_{2,3}$ = 10.5 Hz), 4.91 – 4.86 (m, 2H, H-4), 3.95 (dt, 2H, H-5, $J_{5,6a}$ = 2.5 Hz; $J_{4,5}$ = $J_{5,6b}$ = 9.5 Hz), 3.23 (dd, 2H, H-6a, $J_{6a,6b}$ = 11.0 Hz), 3.06 (dd, 2H, H-6b), 2.14, 2.07. 2.02 (3 s, 19 H, 6 methyl groups). ^{13}C-NMR (125 MHz, $CDCl_3$) δ ppm: 169.92, 169.59,

169.46 (carbonyl groups from acetyl moieties), 91.78 (C-1), 72.35 (C-4), 69.96, 69.76, 69.31 (C-5. C-3, C-2), 21.17, 20.68, 20.62 (methyl groups), 2.44 (C-6). IR: ν_{max} (cm^{-1}) 1742, 1367, 1216, 1028, 656, 593, 566, 558, 528, 513, 493. ESI-MS positive ion mode: calculated m/z $(C_{24}H_{32}O_{15}I_2Na)^+$ ($[M+Na]^+$): 836.9723; found m/z: 836.9721; Δ(m/z):-0.2498 ppm.

2.2.3. Preparation of Hydrogels from Cross-linked Chitosan (CTS), Citric Acid (CA) and Diiodinated Trehalose derivative (CTS_x-CA_{10}-$ITrh_y$)

Ten systems named CTS_x-CA_{10}-$ITrh_y$ were prepared according to the procedure described below (Figure S5). The targeted final CTS concentrations in mass percentages (weight/weight or w/w) were 3%, 4% or 5% w/w and the degree of ionic cross-linking (ion-XrL) was fixed by 10% for all the samples. Finally, the degree of cov-XrL was set at 0%, 5% or 10%. In Table 1 and along the text "x" denotes CTS concentration (% w/w), and "y" denotes the degree of cov-XrL in the hydrogel. The ionic cross-linker was added dissolved in double-distilled water (10 mg/mL concentration), the covalent cross-linker was added in ethanol (50 mg/mL concentration) at 40 °C, and the final mass was adjusted to 25 g with double-distilled water.

The general procedure followed for the preparation of aqueous cross-linked CTS-CA-ITrh conjugates is summarized next (Figure 1, Table S1) and, as an example, the recipe includes the amounts of the reagents necessary for the preparation of sample CTS_4-CA_{10}-$ITrh_5$ (hydrogel with 4% w/w polymer concentration, 10% of degree of ion-XrL and 5% of degree of cov-XrL): CTS with a deacetylation degree of 75% (CTS, 1 g, 4.36 mmol of free amine groups) was charged in a flask provided with a stirrer bar; then, an aqueous solution of citric acid (CA, 2.80 mL, 1% w/v, 0.15 mmol), a solution of di-iodinated trehalose derivative in ethanol (ITrh, 1.78 mL, 5% w/v, 0.11 mmol), a solution of acetic acid (HAc, 0.25 mL, 52% w/v) and double-distilled water (up to a final weight of 25 g, and final polymer concentration of 4% w/w) were added in sequence. Five-minute stirrings were performed between the addition of each reagent. Once all the reagents were added, the mixture was stirred for another 90 min at 40 °C. The solution was cooled to room temperature, the stir bar removed, and stirring proceeded

overnight on a roller at 25 °C. The gelation of the systems was confirmed when the mixtures stopped flowing upon tube inversion for 60 s [23] (Figure S5). Three different batches of these conjugates were synthesized for comparative purposes.

Table 1. *CTS concentration and degree of covalent cross-linking of the 10 CTS-based hydrogels prepared. Rheological parameters.*

Sample	Formulation code	CTS Conc. (%w/w)	Degree cov-Xr (%)	pH	Rheological properties[a]				
					Tan δ (at 1 rad/s)	G'_1 (Pa)	m	K ($Pa \cdot s^n$)	n
1	**CTS_3-CA_{10}-$ITrh_0$**	3%	0	5.6	1.58	10.4	0.70	65.68	0.46
2	**CTS_3-CA_{10}-$ITrh_5$**	3%	5	5.6	1.50	17.2	0.63	43.68	0.50
3	**CTS_3-CA_{10}-$ITrh_{10}$**	3%	10	5.5	1.14	30.7	0.61	61.67	0.50
4	**CTS_4-CA_{10}-$ITrh_0$**	4%	0	5.8	0.87	73.3	0.46	233.97	0.31
5	**CTS_4-CA_{10}-$ITrh_5$**	4%	5	5.5	0.84	121.5	0.42	237.54	0.30
6	**CTS_4-CA_{10}-$ITrh_5$**	4%	5	5.9	0.77	93.1	0.45	251.33	0.30
7	**CTS_4-CA_{10}-$ITrh_{10}$**	4%	10	5.3	0.70	146.0	0.39	324.39	0.22
8	**CTS_5-CA_{10}-$ITrh_0$**	5%	0	6.3	0.68	233.9	0.39	475.41	0.18
9	**CTS_5-CA_{10}-$ITrh_5$**	5%	5	6.2	0.63	249.8	0.33	463.41	0.17
10	**CTS_5-CA_{10}-$ITrh_{10}$**	5%	10	6.3	0.46	653.3	0.29	449.07	0.17

Degree of ionic cross-linking: 10% in every sample;
CTS conc = concentration (in w/w percentage) of CTS;
Degree cov-Xr = degree of covalently cross-linked amino groups in CTS material by diiodo trehalose derivative;
[a]Power-law model parameters and loss tangent at 1 rad/s for CTS_x-CA_{10}-$ITrh_y$ hydrogels studied.

Figure 1. *General procedure for the formation of doubly cross-linked CTS-CA-IThr hydrogels.*

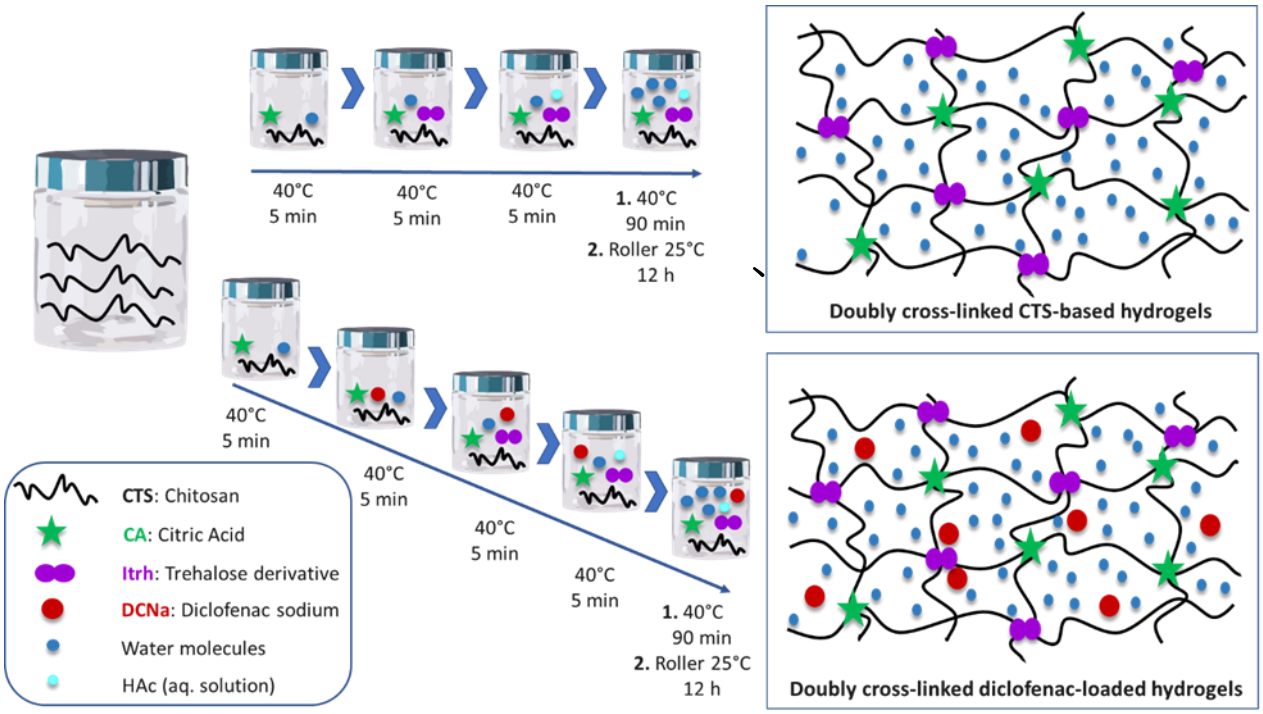

2.2.4. Preparation of Diclofenac Sodium Loaded Formulations from Cross-linked Chitosan-Conjugates

Ten systems named DCNa-CTS_x-$ITrh_y$ were prepared. The preparation process was similar to that of non-loaded hydrogels except that a solution of DCNa in ethanol was added into the mixture just after the ionic cross-linker CA (Figure 1). Final CTS concentrations: 3%, 4% or 5% w/w; degree of ion-XrL: 10%; degree of cov-XrL: 0%, 5% or 10%; final DCNa concentration: 1% w/w.

2.2.5. Hydrogel studies

The dried samples were examined by thermogravimetric analysis (TGA), and the decomposition temperatures were observed. The thermogravimetric analyzer was TA Instruments Q-600 SDT (New Castle, DE, USA). Platinum pans containing approximately 5 mg of each sample were used. Trials were conducted under inert atmosphere (nitrogen, flow rate: 100 mL/min, heating rate: 10°C/min), from 0°C to 700°C.

To measure the pH of the samples, the selected hydrogel (1 g) was placed in a glass container and 10 mL of double-distilled water was added. It was shaken gently and the obtained pHs are shown in Table 1. pH readings of the samples were determined electrometrically using digital pH-meter (HI98103; Hanna Checker pH-meter, Hanna Instruments).

2.2.6. In vitro degradation of CTS_x-CA_{10}-$ITRh_y$ hydrogels

The in vitro degradation studies of hydrogels were conducted following the procedure described by Liu and coworkers for collagen-based hydrogels [36]. Thus, 60-80 mg of hydrated hydrogels (n = 3 of each formulation) were immersed in vials containing 5 mL of 0.1 M PBS (pH 5.7), followed by addition of 30 µl trehalase (2UN/mL). The vials were incubated at 37 °C with shaking at 100 rpm. At different time intervals, the hydrogels were taken out and rinsed with double-distilled water to remove excess salinity. The weight of each sample was measured after all surface water was carefully blotted off. The percent residual mass of hydrogels was calculated according to Equation 1:

$$\text{Residual mass } (\%) = \frac{W_t}{W_0} \text{ x } 100 \qquad \text{(Eq. 1)}$$

where W_0 is the initial weight of the hydrogel and W_t is the weight of the hydrogel at each time point.)

2.2.7. Rheological Studies and Experimental

CTS_x-CA_{10}-$ITrh_y$ hydrogels were rheologically characterized in a controlled-strain (ARES, Rheometric Scientific, Surrey, UK) rheometer, using a serrated plate-plate (25 mm diameter, 1 mm gap) geometry. Small amplitude oscillatory shear (SAOS) tests were carried out inside the linear viscoelastic region in a frequency range of 0.03–100 rad/s at 25 °C. Strain sweep tests were previously performed to determine the linear viscoelastic regime. Viscous flow tests were also made by applying a stepped shear rate ramp in a shear rate range of 0.06–100 s^{-1} at 25 °C. Each fresh sample was tested at least in duplicate. The rheological parameters obtained are recorded in Table 1.

2.2.8. Experimental Model Design for the analysis of rheological parameters

In order to study the influence of CTS concentration and the degree of cov-XrL in the rheological properties of the hydrogels, a Box–Behnken experimental design (CSS Statistica, StatSoft Inc., Tulsa, UK) was used to evaluate the significance of these independent variables as well as the interactions among them in the rheological parameters G'_1, m, tan δ, K and n. The number of experiments (N) is defined by the Equation 2:

$$N = k^2 + k + cp \quad \text{(Eq. 2)}$$

where *k* represents the number of factors (variables) involved in the study and *cp* is the number of replicates of the central point. Box–Behnken could be seen as a cube, consisting of a central point and the middle points of the edges.

The total number of experiments required for our considered independent variables at three levels was 10. The values of the selected pair of independent variables were normalized from -1 to +1 by using Equation 3 in order to facilitate direct comparison of the coefficients and visualization of the effects of the individual independent variables on the response variable.

$$X_n = \frac{X - \bar{X}}{(X_{max} - X_{min})/2} \quad \text{(Eq. 3)}$$

where X_n is the normalized value of independent variables; X is the absolute experimental value of the variable concerned; $\overline{X}$ is the mean of all fixed values for the variable in question; and X_{max} and X_{min} are the maximum and minimum values of the variable, respectively.

2.2.9. Diclofenac Sodium Release Studies

The evaluation of drug release was conducted by ultraviolet-visible (UV-vis) spectroscopy. UV-vis measurements of DCNa-loaded hydrogels were performed with a

Shimadzu UV-2102 PC UV–visible spectrophotometer (Kyoto, Japan). The data were the result of, at least, three measurements.

Prior to the release analyses, a calibration curve of DCNa concentration against absorbance at 280 nm was made with six DCNa standard solutions (buffered solutions at pH 5.5). The equation obtained (Equation 4) determines the linear relationship between UV absorbance (*A*, at 280 nm) and DCNa concentration (C, in mg/mL) in the range of drug concentration studied (from 100 µg/mL to 12.5 µg/mL).

$$A = 27.525\ C + 0.027 \quad \text{(Eq. 4)}$$

The selected hydrogel (1 g) was transferred to a dialysis tubing cellulose membrane (molecular weight cut-off: 8,000–14,000 Da), then immersed in 200 mL of phosphate buffer at pH 5.5 in a round-bottom flask provided with a stirrer bar at 37 °C. At pre-designed time intervals, aliquots were taken from the release medium and the amount of DCNa released was determined by UV–vis spectroscopy at 280 nm. One mL of pre-heated buffer solution was added to the release medium to maintain a constant volume. Experiments were performed in triplicates.

2.2.10. Studies of Hydrogels Morphologies by Scanning Electron Microscopy

The morphologies of selected samples were examined by Scanning Electron Microscopy (SEM) using a field emission scanning electron microscope FEI Teneo. Images were recorded at an accelerating voltage of 5 kV using secondary electrons. Before SEM observations, the hydrogel scaffold was directly frozen at -20 °C for 3 h, then at -80 °C for 24 h [37]. After that, the samples were lyophilized by freeze drying for 24 h. Small pieces of dry hydrogels were cut by razors, then fixed on aluminum stubs using a double-sided carbon tape and finally sputter-coated with about 20 nm of gold.

3. Results and discussion

In the present work we focused on the preparation of CTS-based hydrogels by combining ion-XrL with cov-XrL in order to increase the viscoelastic properties of CTS hydrogels regarding those recently found for ion-XrL hydrogels [17] and study their impact on the

transport of a model anionic API, DCNa. Another parameter to investigate was the effect of an increment in CTS percentages regarding those tested in the previous study as well as the use of another ionic cross-linking agent, CA, which could also enhance hydrogen bonds formation in the hydrogel structure. The impact of this double cross-linking on the release kinetics of the anionic drug will be addressed.

3.1. Preparation of Hydrogels from Cross-linked Chitosan (CTS), Citric Acid (CA) and Diiodinated Trehalose (ITrh) (CTS_x-CA_{10}-$ITrh_y$)

The tricarboxylic ionic cross-linker CA and the electrophile (and covalent cross-linker) derived from α-D-trehalose, the 6,6'-dideoxy-2,3,4,2',3',4'-hexa-*O*-acetyl-6,6'-diiodo-α-D-glucopyranosyl-α-D-glucopyranoside (ITrh), were used to render a new family of doubly-cross-linked hydrogels. The ionic cross-linking agent, CA, allowed the establishment of ionic bonds and hydrogen bonding with the ionized amine groups and the hydroxyl groups from CTS. The cross-linker ITrh, a disaccharide with hydrolyzable glycosidic bond in its structure, was used in aqueous media. This cross-linking agent reacted with the amino groups of the CTS leading to 3D networks, with potential degradable properties under physiological conditions (Scheme 1).

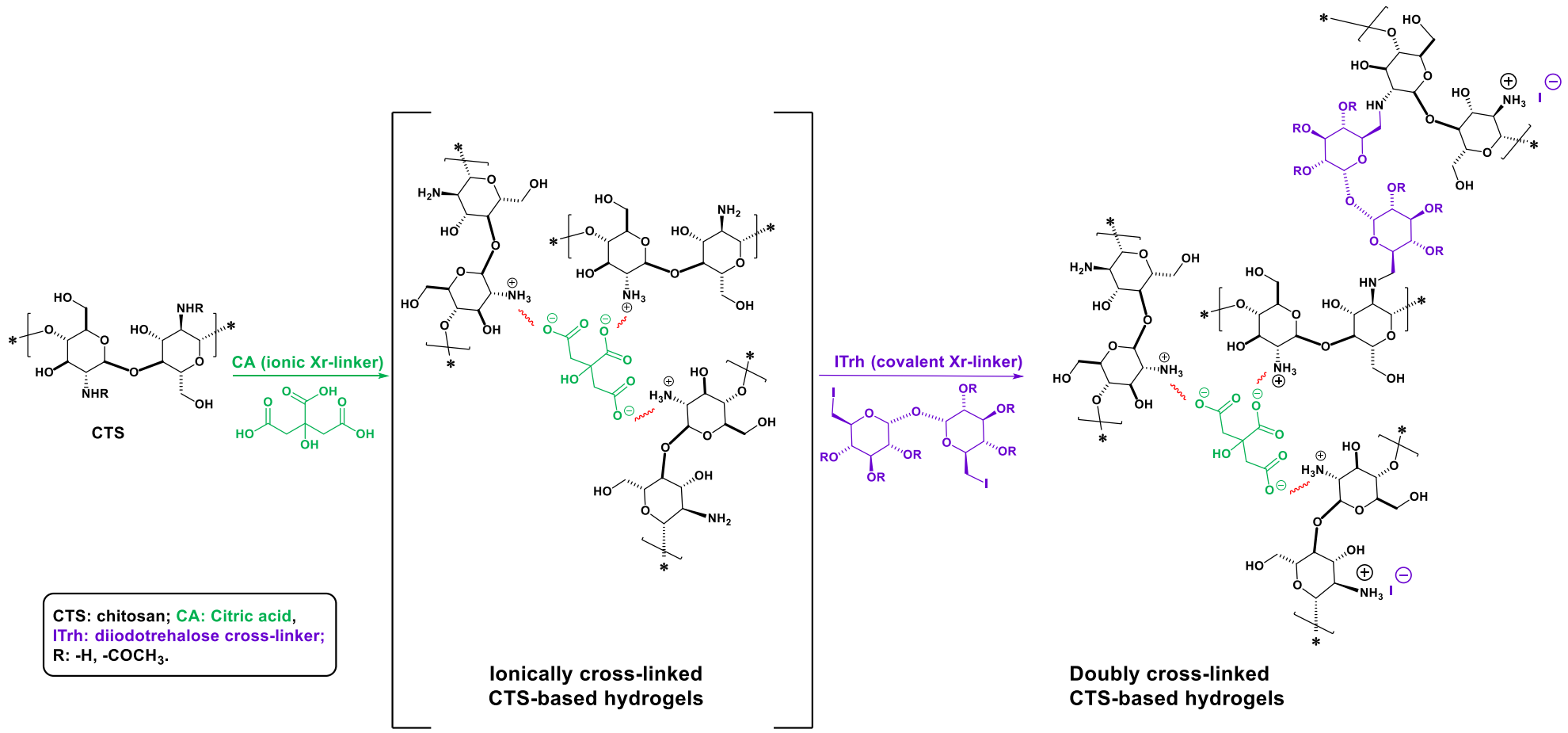

330

331 **Scheme 1**. *Reactions involved in the formation of doubly cross-linked CTS-CA-IThr hydrogels*.

ITrh was synthesized by a modified procedure from Sizovs *et al.* [35]. Due to the symmetrical character of the starting disaccharide material α,α-trehalose, the two iodine groups at C-6 and C-6' could be considered equivalent, and a double reaction with amine groups from CTS was likely to occur.

^{1}H NMR, COSY ^{1}H NMR, ^{13}C NMR and ESI-MS of the diiodo derivative from α-D-trehalose (ITrh) are recorded in Figures S1-S4. Due to the symmetry of the molecule, NMR spectra —mono and two-dimensional ^{1}H,^{13}C and COSY— do not show high complexity. Spectral analyses confirmed the chemical structure of the cross-linker. Thus, the presence of two double doublets at *ca.* 3.2 and 3.1 ppm in the ^{1}H MNR and COSY spectra, correlated to the protons from the iodomethylene units of the glucopyranose rings, should be stood out. It is also noteworthy the presence of a peak at 2.5 ppm in the ^{13}C NMR spectrum associated to the mentioned methylene groups. Moreover, the chemical structure of ITrh was unequivocally confirmed by its Electrospray Ionization (ESI) High Resolution mass spectrum, with a peak at m/z ratio 836.9721, corresponding to $[M+Na]^{+}$ ion.

To confirm the cross-linking in the hydrogels, FTIR spectra of the starting materials and the hydrogels were obtained (Figure 2). Figure 2A records the spectra of the polymer (CTS), the two cross-linkers used (CA and ITrh) and one of the hydrogels formed (CTS_3-CA_{10}-$ITrh_{10}$). In Figures 2B, 2C and 2D, only selected FTIR spectra and sections were recorded.

The existence of ionic cross-linking interactions in CTS-based hydrogels was firstly confirmed (Figure 2B). This ionic interaction occurred because of the acid-base reaction between the carboxylic acid groups from CA and some of the amine groups from CTS. In the CTS FTIR spectrum, O-H bonds from hydroxyl groups provide a broad band centered at 3288 cm^{-1}, which is overlapped with the stretching bands corresponding to the N-H bonds from amine and amide groups. In addition, several significant bands were of interest in the FTIR spectrum of CA. The bands at 3493 and 3276 cm^{-1} (sharp and broad bands, respectively) are mainly due to the stretching of the O-H bonds found in the carboxylic acid groups of CA. Other two bands (1742 and 1692 cm^{-1}), both sharp and intense, can be correlated to the stretching of C=O bonds present in the two types of

carboxylic acid groups of CA. None of these CA bands were present in sample 3 confirming the acid-base reaction mentioned above. In contrast, a new band at 1542 cm^{-1} (stretching band of C=O in carboxylate ions), has emerged as well as a shift of st N-H band, (at 3250 cm^{-1}), in this case correlated with the freshly formed ammonium ions from CTS protonation.

From the chemical point of view, the covalent cross-linking took place by a nucleophilic reaction in which some amine groups of CTS attacked the iodomethylene moieties of ITrh, giving rise to secondary amino groups and iodide ions (Scheme 1). To detect that this cross-linking reaction was successfully accomplished, the disappearance of the stretch band due to the covalent C-I bond in the ITrh cross-linker in the region comprehended between 600 and 400 cm^{-1} was investigated. Figure 2D displayed the IR of sample 3 and ITrh. As can be observed, the bands at 513 and 493 cm^{-1} associated to the stretching of C-I bond [38] in unreacted ITrh were not found in the IR spectrum of sample 3, which is the confirmation that the chemical cross-linking between CTS and ITrh had taken place. It was also noticed that during the gelling procedure (Figure 2C), the labile acetate groups from ITrh were hydrolyzed, as confirmed by the disappearance of the bands at 1741 and 1210 cm-1 (stretching bands of C=O and O-CO bonds, respectively).

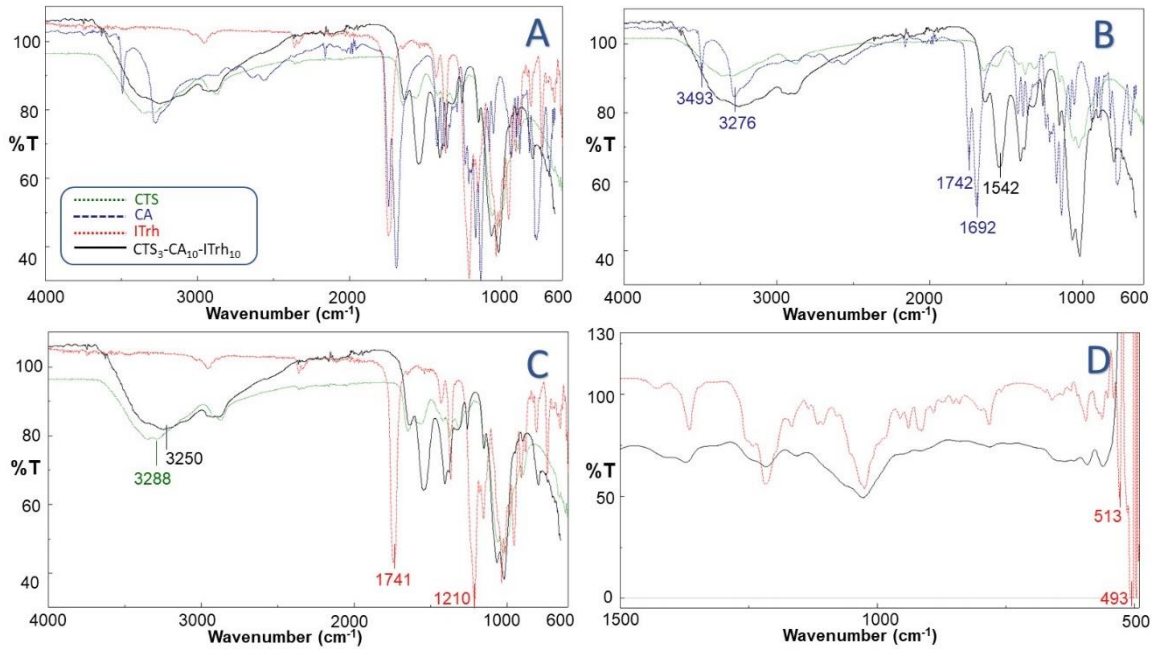

Figure 2. *FTIR spectra of CTS, the cross-linkers used (CA and ITrh) and one of the prepared hydrogels freeze-dried (sample 3: CTS_3-CA_{10}-$ITrh_{10}$). The color code for Figures A, B C and D is as follows: CTS: green; CA: blue; ITrh: red; CTS_3-CA_{10}-$ITrh_{10}$ hydrogel: black. Representative bands have been included.*

An experimental model design was conducted to study the influence of CTS concentration and the degree of cov-XrL on the rheological properties of prepared hydrogels. Ten systems named CTS_x-CA_{10}-$ITrh_y$, in which "x" denotes CTS concentration (% w/w), and "y" denotes the degree of cov-XrL in the hydrogel, were prepared. The targeted final CTS concentrations ranged from 3% to 5% w/w and the degree of cov-XrL varied from 0%, to 10%), setting a degree of ion-XrL of 10% for all the trials (Table 1).

3.2. Thermogravimetric Analyses (TGA)

The thermal stability of the freeze-dried hydrogels was evaluated by thermogravimetry under an inert atmosphere. Characteristic parameters resulting from the experiments are provided in Table S2. Figure S6 displays the TGA curves of CTS, CA and Sample 3 (CTS_3-CA_{10}-$ITrh_{10}$).

The main peak of the thermograms was centered at values close to 300 °C and was associated with the degradation of the cov-XrL ITrh and CTS backbone due to their

structural similarity. The thermo-degradation step centered at 215 °C and characteristic for the ionic cross-linker CA was not observed in the thermograms of CTS-based hydrogels. It could be inferred from this fact that CA is structurally integrated into the hydrogel structures and is exerting its action as cross-linker effectively. This conclusion is supported by the FTIR results already discussed.

On the other hand, and being all the samples highly hydrophilic materials, a weight loss associated to water content was observed for all the formulations at low and high temperatures. This was confirmed by the analyses of their thermograms: weight loss vs temperature and non-reversible heat flow *vs* temperature plots. For both, CTS starting material and hydrogel formulations, there was a clear endothermic event with associated maximum weight loss in the range from 45 °C to 72 °C, probably due to water molecules slightly attached to hydrogel structures [39]. It is remarkable that, after experiencing the same freeze-dry procedure, that water content was substantially higher in the freeze-dried hydrogels than that found in CTS, with increases in *ca*. 67% (water content in CTS: 9%; water content in freeze-dried hydrogels: from 14 to 17%).

Moreover, in the case of hydrogel formulations, a bonus water content (from 7% to 13%) was sustainably detached when heated to values close to 200 °C with maximum weight losses at temperatures between 145 °C and 181 °C and depended on the concentration of CTS: the higher the concentration of CTS, the lower their water content. However, CTS itself showed no weight loss at temperatures ranging from ca. 120 °C to 220 °C. It is hypothesized that water is firmly retained inside the 3D structure of the cross-linked materials. Therefore, the new hydrogels possess enhanced water retention capacity than may be closely related to the presence of more hydrophilic groups, such as $-COO^-$, −COOH, $-NH_3^+$and -OH, available as centers to attract water [40].

3.3. In vitro degradation of CTS_x-CA_{10}-$ITRh_y$ Hydrogels

In general terms, in vitro degradation of polysaccharide-based hydrogels can occur in the polymer backbone through a hydrolytic process that usually causes the breakage of the glycosidic bonds of the polysaccharide chains [41]. In the case of CTS-based hydrogels, hydrolysis takes place either in an acidic medium [42] or mediated by the enzyme lysozyme [43]. Other options are breaking the cross-links and thereby releasing

the biocompatible polysaccharide. In this work, cross-links are the goal of degradation experiments.

The in vitro degradation of the CTS-CA-ITrh hydrogels focused on the lysis of such cross-links by hydrolytic procedures —mediated or not by thehalase— in an acidic microenvironment (pH = 5.7). It was monitored the residual mass percentage of the matrix as a function of time. The reversibility of ionic cross-linking in aqueous media has been well established [25] and hence, a straightforward breakdown of the interactions between CTS and CA was expected. The other cross-linking found in these hydrogels is the trehalose bridges between the CTS chains that were formed during the gelling. These bridges are expected to be degraded by the enzyme trehalase, responsible for the catalytic hydrolysis of the acetal group of trehalose. Under these conditions, certain degree of hydrolysis of the CTS backbone cannot be ruled out.

From the degradation trials, some the samples experienced a water gain in the first few hours, mainly those with higher CTS content, and then a rapid mass loss was observed (from 27 to 54%, depending on the system, Figure 3). This effect could be due to the partial solubilization of the ionic cross-linker in the medium, with the concurrent water loss, causing a loosening of the hydrogel structure. The slower weight loss rates observed for higher cross-linked samples were in line with other authors' observations for covalently cross-linked CTS-based hydrogels [23]. Quasi-plateau regions were observed in the degradation profiles of covalent-cross-linked hydrogels, suggesting a slowdown in their degradation patterns. This could be explained by the need for the enzyme to diffuse into the already eroded hydrogel structure to exert its action.

In intermediate stages of the degradation processes, the most cross-linked systems showed greater hydrolytic stability as demonstrated by Guo and collaborators in the hydrolysis of injectable hydrogels prepared from chitosan-*graft*-polyalanine and oxidized dextran as cross-linker [23]. However, as the degradation experiments progressed, the degradation profiles resembled each other, all being fully disintegrated within 96 h. Trehalose links have demonstrated to be biodegradable under physiological conditions.

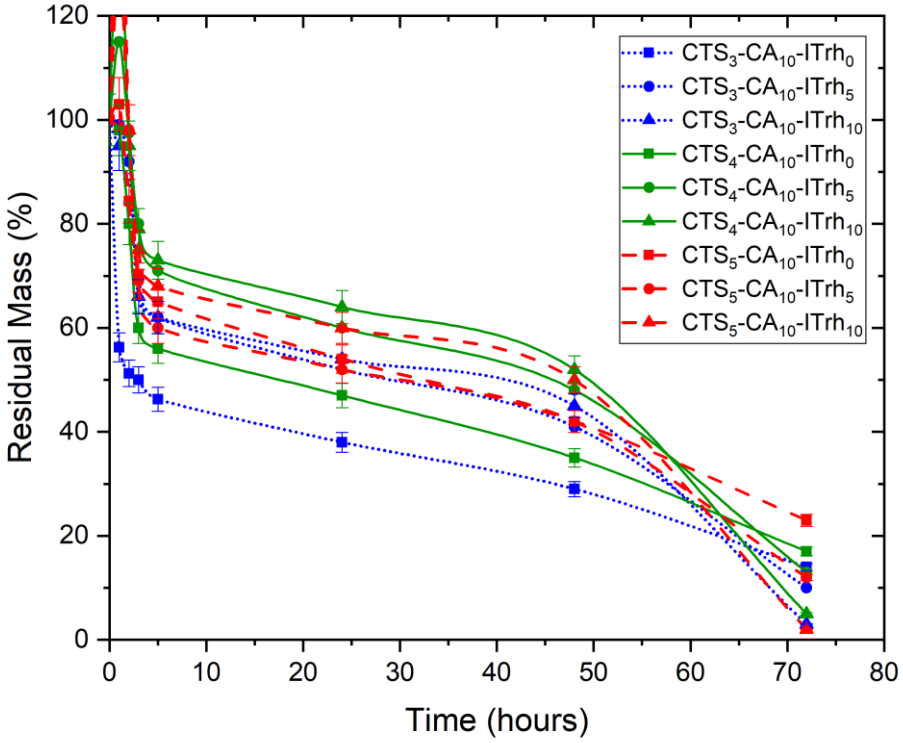

457

458 **Figure 3**. *In vitro degradation patterns of CTS-CA-ITrh hydrogels conducted at pH 5.7 and 37 °C*
459 *in the presence of trehalase. The inset shows the successful biodegradation of the samples under*
460 *the experimental conditions. Error bar: standard deviation (n = 3 different samples for each*
461 *formulation)*

462

463 ### 3.4. Rheological Characterization of CTS_x-CA_{10}-$ITRh_y$ Hydrogels. Correlations
464 ### of Rheological Parameters with CTS Concentration and Degree of
465 ### Covalent Cross-linking Based on an Experimental Model Design

466 The ten hydrogels prepared were rheologically characterized. The influence of CTS
467 concentration and the degree of cov-XrL on significant rheological parameters, such as
468 elastic modulus G', tan δ, consistency, K, and flow, n indexes were mathematically
469 studied by means of Box Behnken experimental designs.

470 Figure 4 shows the evolution of the linear viscoelasticity functions, storage or elastic
471 modulus (G') and loss or viscous modulus (G''), with frequency, as a function of CTS

concentration for samples with ionic degree XrL of 10% and cov-XrL of 5%. As can be observed, it was apparent that an increase in CTS concentration yielded larger figures for the linear viscoelasticity functions as has been demonstrated for other CTS-based hydrogels [20]. The G" values were higher than those found for G' at low CTS concentration and a tendency to reach a crossover point between these functions was obtained at high frequencies. On the other hand, G' values were higher than G" ones at higher CTS concentrations throughout the studied frequency range.

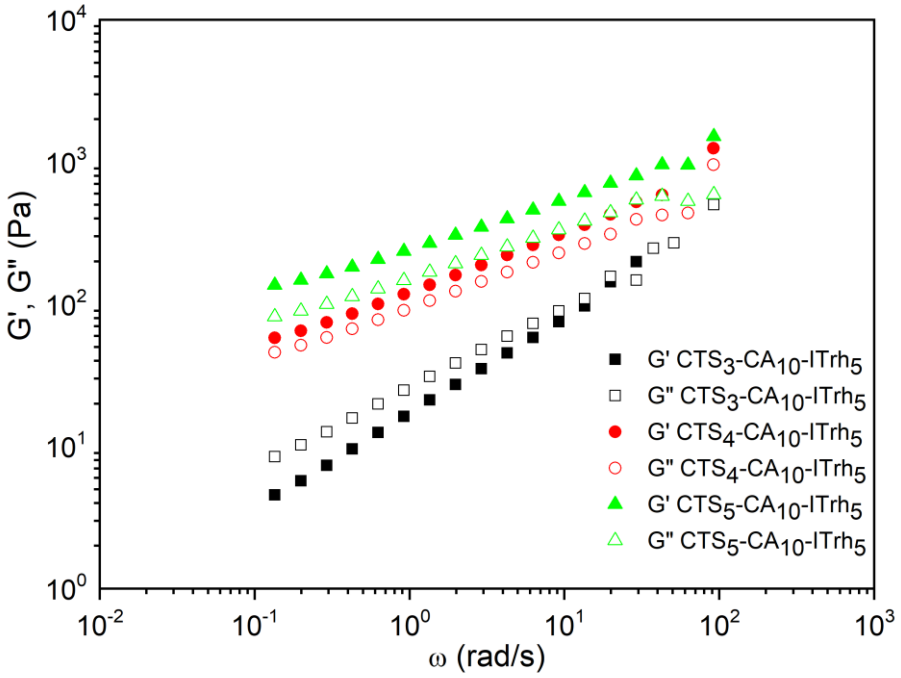

Figure 4. *Frequency dependence of the storage, G', and loss, G", moduli at 25°C, in the linear viscoelasticity region, for hydrogels as a function of CTS concentration.*

Aiming to quantify the dependence on CTS concentration and covalent cross-linked degree, a power-law equation (Equation 5) has been used to describe the evolution of the storage modulus, G', with frequency:

$$G' = G'_1 \, x \, \omega^m \qquad \text{(Eq. 5)}$$

where G'_1 and m are fitting parameters.

Figure 5 illustrates the viscous flow behavior exhibited by selected hydrogels as a function of the degree of cov-XrL. A shear-thinning behavior was apparent in all samples, which could be fitted well to the power-law model (Equation 6):

$$\eta = K \cdot \dot{\gamma}^{n-1} \quad \text{(Eq. 6)}$$

where *K* and *n* are the consistency and flow indexes, respectively. The values of fitting parameters are shown in Table 1. As can be observed an increase in cov-XrL yielded higher viscosity values.

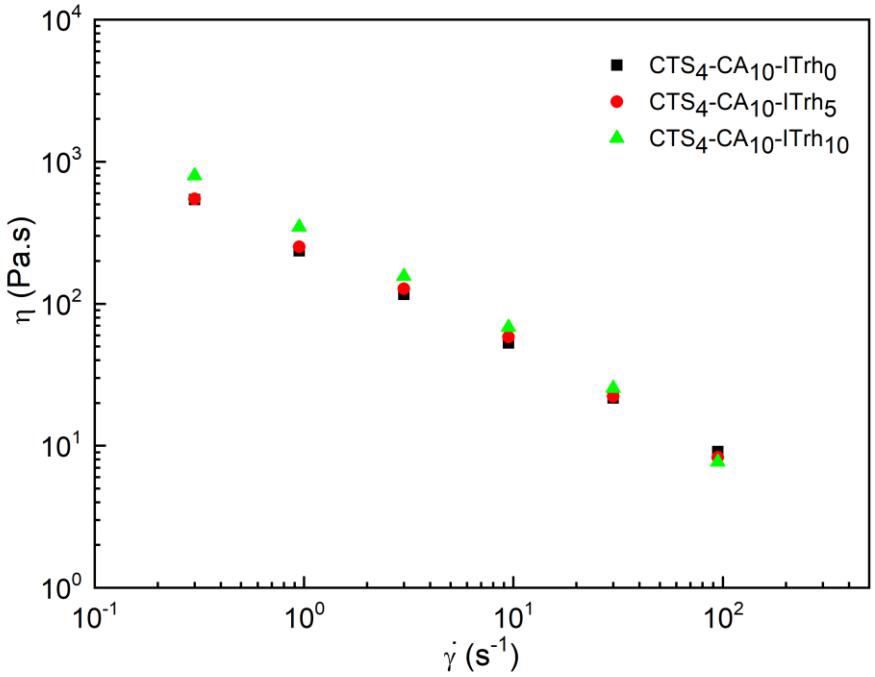

Figure 5. Viscous flow curves for hydrogels, at 25°C, as a function of covalent cross-linked degree.

A Box–Behnken experimental design was used to evaluate the significance of these independent variables (CTS concentration and degree of cov-XrL) related to the rheological parameters recorded in Table 1. In general, for the dependent parameters evaluated in the intervals studied, a greater influence of CTS concentration was observed with respect to that found for the degree of cov-XrL.

In Table 2 the obtained equations by using polynomial regression and the calculated statistics parameters (R^2, d_f and F) are shown. In this sense, a suitable (>0.97) R^2 and (>35) F values have been found in equations.

Table 2. Equations yielded for each dependent variable as a function of the independent variables (normalized values) for the Box-Behnken experimental design.

Equations	R^2	d_f	F
$\boldsymbol{\tan\delta} = 0.838 - 0.41\,[CTS] - 0.146\,Xr + 0.218\,[CTS]^2 - 0.08\,Xr^2 + 0.055\,[CTS]\,Xr$	0.994	5.4	146.32
$\boldsymbol{G'_1(Pa)} = 110.1 + 179.79\,[CTS] + 113.8\,Xr + 109.55\,Xr^2 + 99.78\,[CTS]\,Xr$	0.972	5.4	35.96
$\boldsymbol{m} = 0.427 - 0.155\,[CTS] - 0.0433\,Xr + 0.064\,[CTS]^2$	0.999	3.6	351.08
$\boldsymbol{K(Pa\,s^n)} = 251.49 + 202.81\,[CTS] + 7.87\,Xr^2 - 5.58\,[CTS]\,Xr$	0.999	3.6	712.65
$\boldsymbol{n} = 0.30 - 0.1566\,[CTS] + 0.03\,[CTS]^2 - 0.0125\,[CTS]\,Xr$	0.990	3.6	423.68

[CTS] = CTS concentration (% w/w), normalized value; Xr = degree of covalent cross-linking, normalized value; Tan δ = loss tangent (at 1 rad/s); G'_1 = storage modulus; m = power-law index; *K* (Pa s) = consistency index; n = flow index

To facilitate the identification, that on the selected dependent variable the independent variables are applied, the response surfaces for each dependent variable are shown in Figures 6, 7, S7a and S7b. In a set of hydrogels formed from chitosan-*graft*-polyaniline copolymer cross-linked with oxidized dextran, an increase in storage modulus was observed with the degree of cross-linking [23], similar to what was found for the hydrogels from this study, as shown below.

Figure 6a allows estimating the variation of G'_1, with respect to cov-XrL and CTS concentration, over the range considered. These variations in G'_1 were more pronounced at the highest figures of the independent variables, *i.e.,* at 5% of CTS and 10% of cov-XrL. Moreover, G'_1 was more sensitive to changes in polymer concentration than to the other independent variable. Thus, to obtain hydrogels with high G'_1, it is advisable to operate with high degrees of cov—XrL and high CTS concentrations. On the contrary, the lowest values were found at medium-to-low degrees of cov-XrL and low

CTS concentrations. No significant G'_1 figures have been found at low concentrations. These low G'_1 data were independent of the degree of cov-XrL.

Similar to the findings regarding G'_1, the percentage of cov-XrL displayed lower statistical influence in the power-law index (m) (Figure 6b) than that exerted by CTS rates. Moreover, a similar negative (lower values) statistical influence for cov-XrL was found under high and low CTS concentrations. In this way, the efficient selection of the parameters studied entails the use of high CTS concentration and a high degree of cov-XrL to obtain higher m values, fact that seems to indicate a more developed and complex hydrogel microstructure.

Figure 6a **Figure 6b**

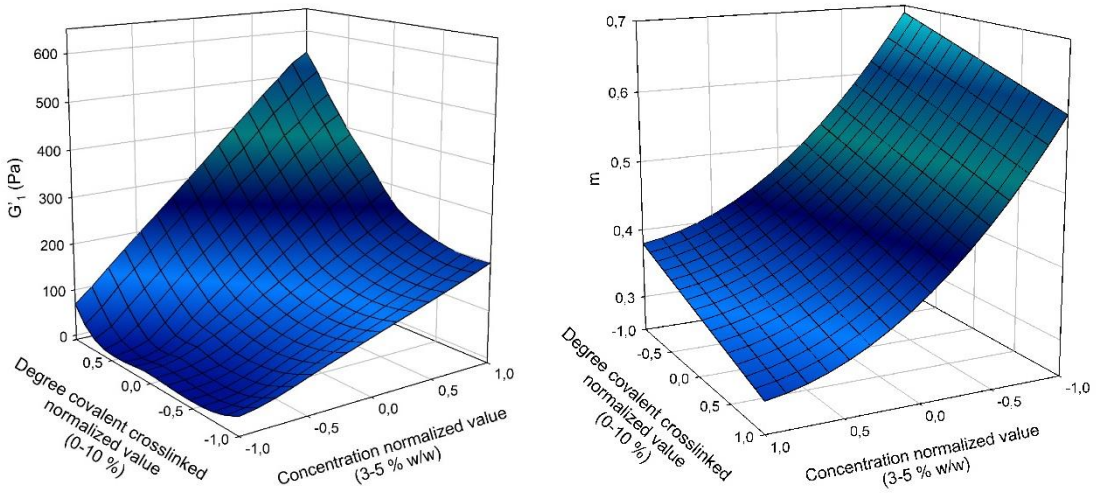

Figure 6. *Response surface models obtained from the Box–Behnken experimental design to evaluate the relative influence of the independent variables (CTS concentration and degree of cov-XrL) on the rheological parameters G'_1 (Fig. 6a) and m (Fig. 6b).*

The response surface for the loss tangent (Tan δ = G''/G') is recorded in Figure 7 to explore the relationships between the independent variables mentioned above and this response variable. Thus, the statistical influences exerted by cov-XrL and CTS concentration followed a similar trend as in the dependent parameters evaluated so far (G'_1, m). Thus, in order to achieve the lowest values for tan δ, the use of high CTS

concentrations and cov-XrL is advisable, indicating that, under these conditions, the relative elastic properties of the hydrogels may increase.

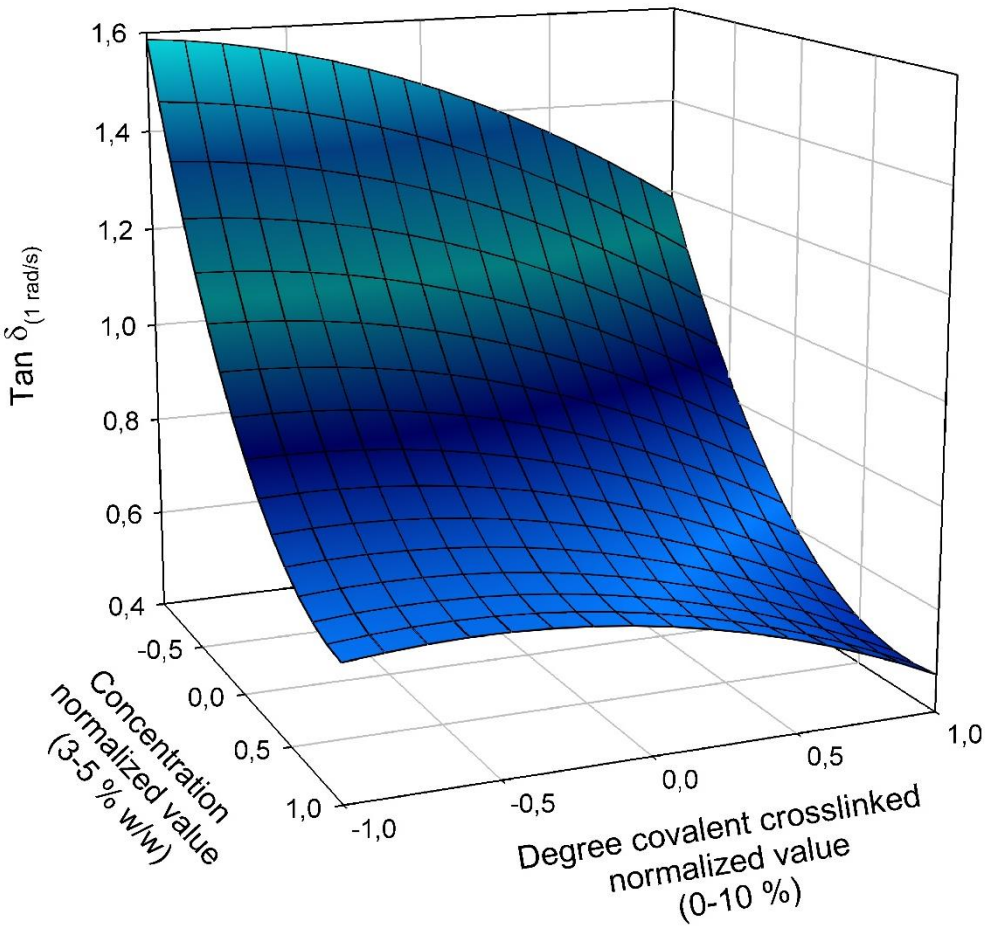

Figure 7. *Response surface model obtained from the Box–Behnken experimental design to evaluate the relative influence of the independent variables (CTS concentration and degree of cov-XrL) on the rheological parameter tan δ at 1 rad/s.*

The consistency index, *K* (Figure S7a) showed a very low statistical dependence on cov-XrL under the studied conditions. Conversely, and regarding polymer concentration, a positive (increasing) statistical correlation was observed, with *K* growing almost linearly with this parameter and hence, the highest values of *K* were found at high CTS concentrations. These results may be explained taking into account that, the structural network of hydrogels became more compact as CTS concentration increased due to the increase in hydrogen bond formation [17], far exceeding the influence that the other

variable can exert. This is also the trend found for flow index (*n*) (Figure S7b). Hence, to obtain the lowest values for *n*, high CTS concentrations should be used.

Therefore, it was concluded that, to achieve hydrogels with maximum elastic properties, the use of high CTS concentrations and high degree of cov-XrL were advisable.

3.5. Diclofenac Sodium Loaded Formulations from Cross-linked Chitosan-Conjugates and Studies of Drug Release

In general terms, and due to the ionizable amino groups present in the polymer backbone, CTS-based hydrogels behave as pH-sensitive DDS, a fact that has been demonstrated in numerous examples such as the release of DOX [8,24], amoxicillin and ibuprofen [23], 5-fluorouracil and diclofenac sodium (DNa) [22] from stabilized CTS-based hydrogels.

Values of pH from 5.5 to 7.5 are within the so-called physiological pH figures in human beings; thus, slightly acidic microenvironments are found in mucous membranes and other topical areas. However, maintaining acid-base balance is critical for the survival of living species since cellular processes are highly sensitive to changes in proton concentrations. Although in humans, pH varies within a narrow range (in the blood between pH 7.35 and 7.45), local deviations from the systemic pH are often caused by pathologies, such as cancer, inflammation, infection, ischemia, renal failure or pulmonary disease [44]. Therefore, drug delivery systems capable of releasing the active pharmaceutical ingredient at acidic pH, such as the formulations studied herein, could find significant applications in a wide range of pathologies and locations.

Sodium diclofenac (DCNa) is one of the most frequently used non-steroidal anti-inflammatory drugs (NSAID) used to treat pain and inflammatory diseases [45]. Because of the short half-life in plasma (1–2 h) and associated adverse effects [46], it is regarded as an ideal model drug for controlled delivery system [22]. DCNa-loaded hydrogels may have potential applications in the treatment of inflammatory bowel disease (IBD), pathologies of great impact in developed countries [26]. For that use, they may release the drug at the acidic pH typical of inflamed areas and even the small intestine (pH 5-

578 7.5) [47–49], and therefore, the release studies of the prepared formulations have been
579 conducted at pH 5.5.

580 As in the study for the rheological properties, ten drug-loaded hydrogel formulations
581 named DCNa-CTS_x-$ITrh_y$ were prepared and are recorded in Table S3. Several examples
582 of formulations of DCNa and CTS have been published, mainly beads, microparticles and
583 hydrogels. For example, the preparation of DCNa-loaded CTS microspheres by double
584 physical emulsification have been described [45] as well as ionically cross-linked
585 DCNa-loaded CTS-based beads was prepared using sodium polyphosphate as a cross-
586 linker. In this case, controlled drug release was confirmed at pH 7.2 and was depended
587 on several formulation factors, such as CTS concentration, drug-polymer ratio and
588 percentage of Tween 80 [50]. The role of silica matrices in DDS has also been explored.
589 DCNa-loaded silica-CTS composites —some of them cross-linked with glutaraldehyde—
590 have been developed to achieve efficient sustained drug-release systems. In this case,
591 the protonated chitosan spheres, were the systems that better controlled the release of
592 DCNa [51]. Regarding gelling systems, Zhang *et al*. prepared DCNa-loaded hydrogels
593 based on carboxymethyl chitosan-*graft*-poly (*N*-isopropyl acrylamide)-glycidyl
594 methacrylate by UV cross-linking. Their findings highlighted that the drug release
595 kinetics depended on pH and temperature. However, the degradability of the networks
596 was not proved for these systems [22]. We have previously investigated the formation
597 of DCNa-loaded ionotropic CTS-based hydrogels in which the drug release and the
598 rheological properties of the systems were strongly dependent on the formulation [17].
599 Unfortunately, the consistency of the prepared matrices ranged from liquid-like to
600 viscoelastic gels. With the aim to improve the physical properties of the materials, in the
601 present study the concentration of CTS has been increased, an additional covalent cross-
602 linking introduced, and the ionic cross-linker replaced by a more hydrophilic molecule.

603 In order to check the release of the DCNa-loaded hydrogels, a calibration curve of the
604 drug was made with DCNa standard solutions at 280 nm [17]. From the samples studied,
605 it was observed that all the hydrogels were able to control the DCNa release for long
606 periods at 37 °C in phosphate buffer at pH 5.5 (Table S3, Figures 8a and 8b). The drug
607 was released in a slow and sustained manner, ranging from 17% to 40% after 72 h. These

enhanced retention figures found for the described DCNa formulations were in concordance with the expected results since the anionic drug could be ionically anchored to the cationic CTS-based hydrogels [7].

The influence of two factors, CTS concentration and the degree of cov-XrL, on the release profiles was studied. When the role played by CTS concentration on DCNa release was investigated, the other variables, degree of ionic XrL and cov-XrL were set at 10%, and 5% respectively. The results are recorded in Figure 8a.

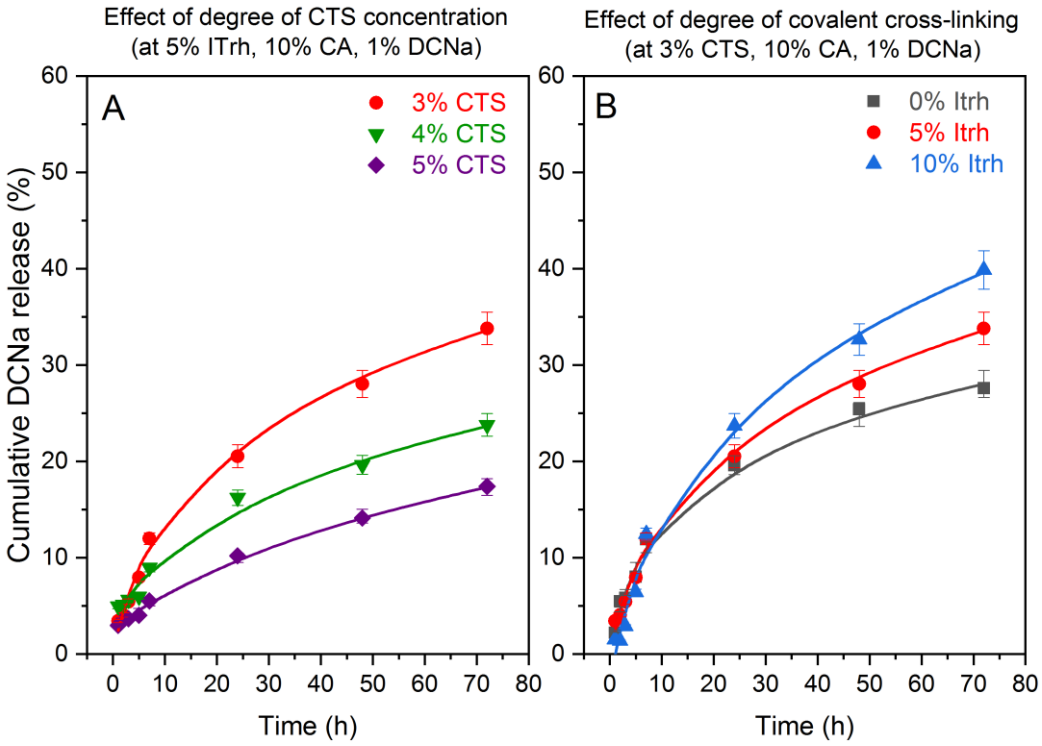

Figure 8. *In vitro release profiles of diclofenac sodium (DCNa) from CTS hydrogels in phosphate buffer solution at pH 5.5 at 37 °C. Data were obtained from UV-Vis spectroscopy at 280 nm and reported as mean ± S.D from three independent experiments. (Fig. 8A) Effect of CTS concentration — from 3% to 5% CTS concentration — in drug release (fixed paraments: degree of covalent cross-linking 5%; degree of ionic cross-linking 10%; DCNa concentration 1%). (Fig. 8B) Effect of degree of covalent cross-linking — from non-cross-linked samples to 10% of cross-linked — in drug release (fixed paraments: CTS concentration 3%; ionic cross-linking 10%; DCNa concentration 1%).*

It was noted that the greatest changes in DCNa release were found among those formulations with the largest differences in the starting-hydrogels rheological behaviors. For example, for the DCNa-CTS_5-$ITrh_5$ sample, the DCNa released after 72 h was only the 17% of the drug present in the formulation. This could be due to the more developed and complex hydrogel microstructures characteristic of the prepared dispersions with the highest CTS content, as the previous rheological studies had demonstrated. When comparing these findings with the drug release from the DCNa-CTS_3-$ITrh_5$ sample, it was observed that the percentage of drug delivered by the latter was two-fold the figure of DCNa released from the DCNa-CTS_5-$ITrh_5$ sample. Consequently, the higher the CTS concentration in the hydrogels, the lower the drug release kinetics. The same trend was reported for disulfide-cross-linked CTS-based hydrogels [7].

Figure 8b shows the release kinetics from selected drug-loaded hydrogels in order to study the impact of cov-XrL on drug release. On the formulations linked to the displayed curves, the degree of ionic XrL was set at 10% for all samples, the percentage of CTS at 3% and the concentration of the drug in the formulations at 1%. Although initially surprising, and being the other parameters constant, drug release was enhanced in the most cross-linked systems (cov-XrL: 10%) leading to a boost in drug release. For example, the percentage of DCNa delivered (after 72 h) were 28% and 40% for samples DCNa-CTS_3-$ITrt_0$ and DCNa-CTS_3-$ITrt_{10}$, respectively. This assessment related to the influence of cov-XrL in cumulative drug release was accurate for all the formulations studied regardless CTS percentage (Table S3). This trend has also been observed for the release of amoxicillin from CTS-oxidized dextrin hydrogels. Other authors reported that when the cross-linking density of the hydrogels increased, the rate of drug release also augmented. They explained this observation based on the fact that hydrogels with higher cross-linking density would have swelled less, thus causing a higher concentration gradient of the drug. [23] Another hypothesis could be that either the bulky trehalose units between the CTS chains or the volatile solvent used in the preparation of the formulations [52] had behaved as a porogen and may have altered, to some extent, the regular packaging of the CTS in the material. This outcome could have generated interconnected pores that allowed the penetration of water molecules into the matrices, modifying the overall drug release rates due to the generation of drug release

channels [53]. Therefore, the higher the degree of cov-XrL, the greater the free volume found in the matrices, and hence, the faster the drug would diffuse into the medium. This assumption was supported by the SEM images found for DCNa-loaded hydrogels at 4% of CTS.

These findings suggested that the prepared hydrogels can not only act as DDS but can also be used to tune the rate of drug release by changing the degree of cross-linking [8], and/or by modifying the polymer concentration. It is anticipated that the release of non-ionic drugs will show a faster kinetics than those exhibited by the anionic drug DCNa, as it was the case in disulfide-cross-linked CTS-based hydrogels [7].

3.6. Scanning Electron Microscopy (SEM) Studies

The SEM micrographs displayed in Figures 9a and 9b show the scaffolds of CTS-CA-ITrh and DCNa-CTS-ITrh hydrogels (before and after DCNa loading, respectively) at different CTS concentrations and degrees of cov-XrL. As can be observed in Figure 9a, CTS-CA-ITrh hydrogels prepared with CTS ≤ 4% and XrL ≤ 5% displayed scaffolds with well-defined lamellar structures. At higher CTS contents, such structures tended to disappear in favor of more compact scaffolding. When the degree of cov-XrL reached 10%, matrices containing small pores were found. Similarly to other findings previously reported by us [17], the presence of DCNa caused a change in the morphologies of the hydrogels (Figure 9b) and led to more porous microstructures than their non-loaded counterparts. The role of DCNa as a porogen in the hydrogels is hypothesized. For DCNa-CTS-ITrh hydrogels, the lower the percentages of CTS, the greater and larger the number of pores found. These observations are consistent with both the rheological properties of the precursor hydrogels. Evidence of larger number of interconnected pores at low CTS percentages also supports the faster DCNa release found for DCNa-CTS_3-ITrh formulations. It has been demonstrated that interconnected pores may significantly reduce the diffusion length for drug release and the volume fraction of polymer [42]. Thus, DCNa-loaded hydrogels prepared with the highest CTS concentration exhibited a developed and complex hydrogel microstructure, responsible for the retention of the anionic drug in the gel-like matrices. The release studies confirmed that the increase in the percentage of CTS decreased the rate of drug release in all the samples studied.

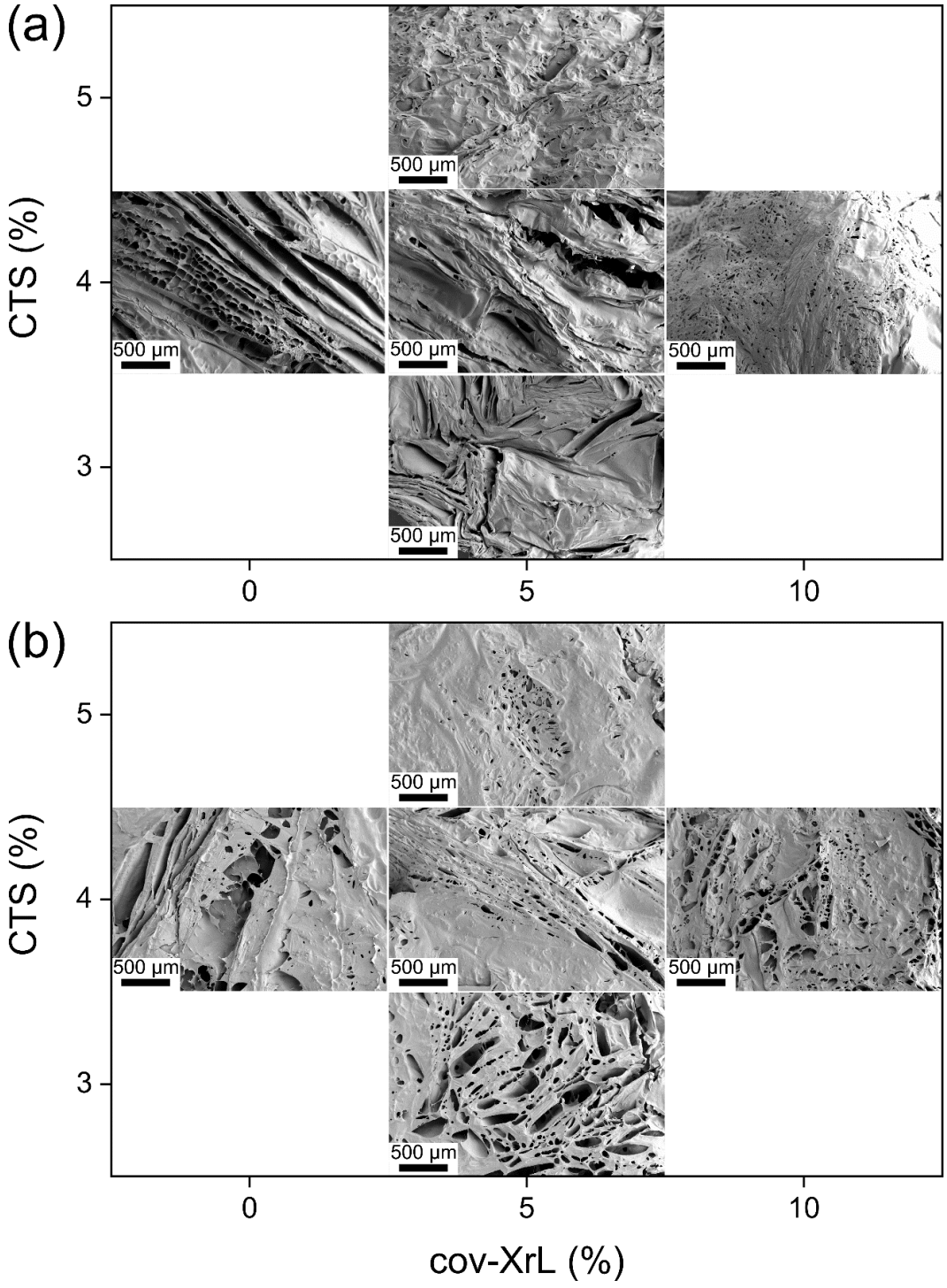

685

686 **Figure 9.** *SEM micrographs showing the scaffolds evolution of (a) CTS-CA-ITrh and (b) DCNa-*
687 *CTS-ITrh hydrogels at different CTS concentrations and degrees of cov-XrL. For comparison*
688 *purpose, all the images were recorded at the same magnification.*

689 To sum up, all drug-loaded hydrogels displayed a controlled and steadily DCNa release
690 at 37 °C with cumulative release figures ranging from 17% to 40% after 72 h. To what

extent the drug release occurred was strongly dependent on the composition of the formulation.

In despite of the relevant morphological changes observed by SEM in DCNa-loaded and non-loaded hydrogels, it was clear that the ionic interactions established between the anionic drug and the cationic matrices was a relevant parameter regarding drug release. The high percentage of CTS in the systems contributed to a more densely 3D ionic anchoring of DCNa, decelerating the drug release. It is anticipated that the release of non-ionic drugs will show faster kinetics than those exhibited by anionic APIs.

4. Conclusions

The preparation of a new family of eco-friendly and biodegradable chitosan-based hydrogels have been successfully achieved by means of ionic and covalent cross-linking (ion-XrL and cov-XrL). The novel hydrogels completely disintegrated within 96 h by means of a hydrolysis process mediated by the enzyme trehalase. As far as the authors are aware, this is the first time that a trehalose derivative has been used as a covalent cross-linker in the formation of biodegradable hydrogels, converging the improved physical properties of stable hydrogels with the inherent degradability of ionotropic hydrogels.

Through an experimental model design, the influence of two parameters —polymer concentration and degree of cov-XrL— on hydrogel rheological properties was disclosed, being the former the most influential variable. Hydrogels with maximum elastic properties were achieved at the highest CTS concentrations and degrees of cov-XrL. These moduli agreed with the scaffold morphologies found by SEM micrographs in which the hydrogels prepared with lower CTS content and lower degree of cov-XrL showed well-defined lamellar structures, whereas at higher CTS and cov-XrL, such structures evolved to more compact scaffolding.

Ten DCNa-containing formulations with different polymer concentration, and degree of cov-XrL were evaluated regarding their release profiles. They displayed well-controlled drug-release patterns that were strongly dependent on the formulation composition,

719 with cumulative drug release varying from 17% to 40% for 72 h under physiological
720 conditions. Systems with improved viscoelastic properties exhibited the lowest rates of
721 drug release. Surprisingly, a boost in drug release was found in those formulations with
722 the highest levels of covalent cross-linking. This trend could be extrapolated to any CTS
723 concentration value.

724 In summary, the preparation method of the CTS-based drug formulations presented
725 herein provides a simple and straightforward pathway to design tailor-made controlled
726 drug delivery systems with improved rheological properties. Their degradability bears
727 real relevance to their potential use in biomedical applications. We anticipate that these
728 systems can be readily adapted to achieve effective encapsulation of other APIs of
729 interest for sustained release.

730 Acknowledgments

731 The authors would like to thank *El Ministerio de Ciencia, Innovación y Universidades*
732 (MICINN) of Spain (Grant MAT2016-77345-C3-2-P), and *La Junta de Andalucía* (Grant
733 P12-FPM-1553) for their financial support.

734 References

735 [1] P.M. Favi, R.S. Benson, N.R. Neilsen, R.L. Hammonds, C.C. Bates, C.P. Stephens,
736 M.S. Dhar, Cell proliferation, viability, and in vitro differentiation of equine
737 mesenchymal stem cells seeded on bacterial cellulose hydrogel scaffolds,
738 Materials Science and Engineering C. 33 (2013) 1935–1944.
739 doi:10.1016/j.msec.2012.12.100.

740 [2] L. Liu, Q. Gao, X. Lu, H. Zhou, In situ forming hydrogels based on chitosan for drug
741 delivery and tissue regeneration, Asian Journal of Pharmaceutical Sciences. 11
742 (2016) 673–683. doi:10.1016/j.ajps.2016.07.001.

743 [3] N. Annabi, A. Tamayol, J.A. Uquillas, M. Akbari, L.E. Bertassoni, C. Cha, G. Camci-
744 Unal, M.R. Dokmeci, N.A. Peppas, A. Khademhosseini, 25th anniversary article:
745 Rational design and applications of hydrogels in regenerative medicine, Advanced

746 Materials. 26 (2014) 85–124. doi:10.1002/adma.201303233.

747 [4] M.A. Amin, I.T. Abdel-Raheem, Accelerated wound healing and anti-inflammatory
748 effects of physically cross linked polyvinyl alcohol-chitosan hydrogel containing
749 honey bee venom in diabetic rats, Archives of Pharmacal Research. 37 (2014)
750 1016–1031. doi:10.1007/s12272-013-0308-y.

751 [5] Y. Liu, S. Hsu, Synthesis and Biomedical Applications of self-healing hydrogels,
752 Frontiers in Chemistry. 6 (2018) 449(1–10). doi:10.3389/fchem.2018.00449.

753 [6] N. Bhattarai, J. Gunn, M. Zhang, Chitosan-based hydrogels for controlled,
754 localized drug delivery, Advanced Drug Delivery Reviews. 62 (2010) 83–99.
755 doi:10.1016/j.addr.2009.07.019.

756 [7] M.J. Lucero, C. Ferris, C.A. Sanchez-Gutierrez, M.R. Jimenez-Castellanos, M.-V. de-
757 Paz, Novel aqueous chitosan-based dispersions as efficient drug delivery systems
758 for topical use. Rheological, textural and release studies., Carbohydrate Polymers.
759 151 (2016) 692–699. doi:10.1016/j.carbpol.2016.06.006.

760 [8] Y. Liang, X. Zhao, P.X. Ma, B. Guo, Y. Du, X. Han, pH-responsive injectable
761 hydrogels with mucosal adhesiveness based on chitosan-grafted-dihydrocaffeic
762 acid and oxidized pullulan for localized drug delivery, Journal of Colloid and
763 Interface Science. 536 (2019) 224–234. doi:10.1016/j.jcis.2018.10.056.

764 [9] W.E. Hennink, C.F. van Nostrum, Novel crosslinking methods to design hydrogels,
765 Advanced Drug Delivery Reviews. 64 (2012) 223–236.
766 doi:10.1016/j.addr.2012.09.009.

767 [10] S.A. Shah, M. Sohail, M.U. Minhas, Nisar-ur-Rehman, S. Khan, Z. Hussain,
768 Mudassir, A. Mahmood, M. Kousar, A. Mahmood, pH-responsive CAP-co-
769 poly(methacrylic acid)-based hydrogel as an efficient platform for controlled
770 gastrointestinal delivery: fabrication, characterization, in vitro and in vivo toxicity
771 evaluation, Drug Delivery and Translational Research. 9 (2019) 555–577.
772 doi:10.1007/s13346-018-0486-8.

773 [11] S.K. Shukla, A.K. Mishra, O. a. Arotiba, B.B. Mamba, Chitosan-based
774 nanomaterials: A state-of-the-art review, International Journal of Biological
775 Macromolecules. 59 (2013) 46–58. doi:10.1016/j.ijbiomac.2013.04.043.

776 [12] D. Enescu, C.E. Olteanu, Functionalized Chitosan and Its Use in Pharmaceutical,
777 Biomedical, and Biotechnological Research, Chemical Engineering
778 Communications. 195 (2008) 1269–1291. doi:10.1080/00986440801958808.

779 [13] B. Qu, Y. Luo, Chitosan-based hydrogel beads: Preparations, modifications and
780 applications in food and agriculture sectors – A review, International Journal of
781 Biological Macromolecules. 152 (2020) 437–448.
782 doi:10.1016/j.ijbiomac.2020.02.240.

783 [14] A. Rafique, K.M. Zia, M. Zuber, S. Tabasum, Chitosan functionalized poly (vinyl
784 alcohol) for prospects biomedical and industrial applications : A review,
785 International Journal of Biological Macromolecules. 87 (2016) 141–154.
786 doi:10.1016/j.ijbiomac.2016.02.035.

787 [15] R. Vivek, R. Thangam, V. Nipunbabu, T. Ponraj, S. Kannan, Oxaliplatin-chitosan
788 nanoparticles induced intrinsic apoptotic signaling pathway: A “smart” drug
789 delivery system to breast cancer cell therapy, International Journal of Biological
790 Macromolecules. 65 (2014) 289–297. doi:10.1016/j.ijbiomac.2014.01.054.

791 [16] Y. Xu, J. Han, H. Lin, Fabrication and characterization of a self-crosslinking chitosan
792 hydrogel under mild conditions without the use of strong bases, Carbohydrate
793 Polymers. 156 (2017) 372–379. doi:10.1016/j.carbpol.2016.09.046.

794 [17] N. Iglesias, E. Galbis, C. Valencia, M.-V. De-Paz, J.A. Galbis, Reversible pH-sensitive
795 chitosan-based hydrogels. Influence of dispersion composition on rheological
796 properties and sustained drug delivery, Polymers. 10 (2018) 1–17.
797 doi:10.3390/polym10040392.

798 [18] A. Chenite, C. Chaput, D. Wang, C. Combes, M.. Buschmann, C.. Hoemann, J..
799 Leroux, B.. Atkinson, F. Binette, A. Selmani, Novel injectable neutral solutions of
800 chitosan form biodegradable gels in situ, Biomaterials. 21 (2000) 2155–2161.
801 doi:10.1016/S0142-9612(00)00116-2.

802 [19] Y. Xu, C. Zhan, L. Fan, L. Wang, H. Zheng, Preparation of dual crosslinked alginate-
803 chitosan blend gel beads and in vitro controlled release in oral site-specific drug
804 delivery system, International Journal of Pharmaceutics. 336 (2007) 329–337.
805 doi:10.1016/j.ijpharm.2006.12.019.

806 [20] C. Ferris, M. Casas, M.J. Lucero, M. V de Paz, M.R. Jimenez-Castellanos, Synthesis
807 and characterization of a novel chitosan-N-acetyl-homocysteine thiolactone
808 polymer using MES buffer., Carbohydrate Polymers. 111 (2014) 125–132.
809 doi:10.1016/j.carbpol.2014.03.078.

810 [21] M. Dash, F. Chiellini, R.M. Ottenbrite, E. Chiellini, Chitosan - A versatile semi-
811 synthetic polymer in biomedical applications, Progress in Polymer Science
812 (Oxford). 36 (2011) 981–1014. doi:10.1016/j.progpolymsci.2011.02.001.

813 [22] L. Zhang, L. Wang, B. Guo, P.X. Ma, Cytocompatible injectable carboxymethyl
814 chitosan/N-isopropylacrylamide hydrogels for localized drug delivery,
815 Carbohydrate Polymers. 103 (2014) 110–118. doi:10.1016/j.carbpol.2013.12.017.

816 [23] J. Qu, X. Zhao, P.X. Ma, B. Guo, Injectable antibacterial conductive hydrogels with
817 dual response to an electric field and pH for localized “smart” drug release, Acta
818 Biomaterialia. 72 (2018) 55–69. doi:10.1016/j.actbio.2018.03.018.

819 [24] J. Qu, X. Zhao, P.X. Ma, B. Guo, pH-responsive self-healing injectable hydrogel
820 based on N-carboxyethyl chitosan for hepatocellular carcinoma therapy, Acta
821 Biomaterialia. 58 (2017) 168–180. doi:10.1016/j.actbio.2017.06.001.

822 [25] R. Dong, Y. Pang, Y. Su, X. Zhu, Supramolecular hydrogels: synthesis, properties
823 and their biomedical applications, Biomaterials Science. 3 (2015) 937–954.
824 doi:10.1039/c4bm00448e.

825 [26] N. Iglesias, E. Galbis, M.J. Díaz-Blanco, R. Lucas, E. Benito, M.V. De-Paz,
826 Nanostructured Chitosan-based biomaterials for sustained and colon-specific
827 resveratrol release, International Journal of Molecular Sciences. 20 (2019) 398 (1–
828 16). doi:10.3390/ijms20020398.

829 [27] J. Zhao, X. Zhao, B. Guo, P.X. Ma, Multifunctional interpenetrating polymer
830 network hydrogels based on methacrylated alginate for the delivery of small
831 molecule drugs and sustained release of protein, Biomacromolecules. 15 (2014)
832 3246–3252. doi:10.1021/bm5006257.

833 [28] J. Berger, M. Reist, J.M. Mayer, O. Felt, N.A. Peppas, R. Gurny, Structure and
834 interactions in covalently and ionically crosslinked chitosan hydrogels for
835 biomedical applications, European Journal of Pharmaceutics and

836 Biopharmaceutics. 57 (2004) 19–34. doi:10.1016/S0939-6411(03)00161-9.

837 [29] L. Zhuang, X. Zhi, B. Du, S. Yuan, Preparation of Elastic and Antibacterial Chitosan-
838 Citric Membranes with High Oxygen Barrier Ability by in Situ Cross-Linking, ACS
839 Omega. 5 (2020) 1086–1097. doi:10.1021/acsomega.9b03206.

840 [30] D. Bao, M. Chen, H. Wang, J. Wang, C. Liu, R. Sun, Preparation and
841 characterization of double crosslinked hydrogel films from
842 carboxymethylchitosan and carboxymethylcellulose, Carbohydrate Polymers.
843 110 (2014) 113–120. doi:10.1016/j.carbpol.2014.03.095.

844 [31] D. Ailincai, L. Marin, S. Morariu, M. Mares, A.C. Bostanaru, M. Pinteala, B.C.
845 Simionescu, M. Barboiu, Dual crosslinked iminoboronate-chitosan hydrogels with
846 strong antifungal activity against Candida planktonic yeasts and biofilms,
847 Carbohydrate Polymers. 152 (2016) 306–316. doi:10.1016/j.carbpol.2016.07.007.

848 [32] S. Doppalapudi, A. Jain, W. Khan, A.J. Domb, Biodegradable polymers-an
849 overview, Polymers for Advanced Technologies. 25 (2014) 427–435.
850 doi:10.1002/pat.3305.

851 [33] T. Sun, Y.S. Zhang, B. Pang, D.C. Hyun, M. Yang, Y. Xia, Engineered nanoparticles
852 for drug delivery in cancer therapy, Angewandte Chemie - International Edition.
853 53 (2014) 12320–12364. doi:10.1002/anie.201403036.

854 [34] N. Zhang, H. Zhang, R. Li, Y. Xing, Preparation and adsorption properties of citrate-
855 crosslinked chitosan salt microspheres by microwave assisted method,
856 International Journal of Biological Macromolecules. 152 (2020) 1146–1156.
857 doi:10.1016/j.ijbiomac.2019.10.203.

858 [35] A. Sizovs, L. Xue, Z.P. Tolstyka, N.P. Ingle, Y. Wu, M. Cortez, T.M. Reineke,
859 Poly(trehalose): Sugar-Coated Nanocomplexes Promote Stabilization and
860 Effective Polyplex-Mediated siRNA Delivery, Journal of the American Chemical
861 Society. 135 (2013) 15417–15424. doi:10.1021/ja404941p.

862 [36] W. Liu, C. Deng, C.R. McLaughlin, P. Fagerholm, N.S. Lagali, B. Heyne, J.C. Scaiano,
863 M.A. Watsky, Y. Kato, R. Munger, N. Shinozaki, F. Li, M. Griffith, Collagen-
864 phosphorylcholine interpenetrating network hydrogels as corneal substitutes,
865 Biomaterials. 30 (2009) 1551–1559. doi:10.1016/j.biomaterials.2008.11.022.

866 [37] B. Palma Santana, F. Nedel, C. Perelló Ferrúa, R. Marques e Silva, A. Fernandes da
867 Silva, N.L. Fernando Demarco, Flávio Villarreal Carreño, Comparing different
868 methods to fix and to dehydrate cells on alginate hydrogel scaffolds using
869 scanning electron microscopy, Microscopy Research and Technique. 78 (2015)
870 553–561. doi:10.1002/jemt.22508.

871 [38] R.H. Schuler, The effect of iodine on the infrared spectra of the alkyl iodides, The
872 Journal of Chemical Physics. 22 (1954) 947. doi:10.1063/1.1740227.

873 [39] S. Iravani, C.S. Fitchett, D.M.R. Georget, Physical characterization of arabinoxylan
874 powder and its hydrogel containing a methyl xanthine, Carbohydrate Polymers.
875 85 (2011) 201–207. doi:10.1016/j.carbpol.2011.02.017.

876 [40] H.A. Essawy, M.B.M. Ghazy, F.A. El-Hai, M.F. Mohamed, Superabsorbent
877 hydrogels via graft polymerization of acrylic acid from chitosan-cellulose hybrid
878 and their potential in controlled release of soil nutrients, International Journal of
879 Biological Macromolecules. 89 (2016) 144–151.
880 doi:10.1016/j.ijbiomac.2016.04.071.

881 [41] M. Naveed, L. Phil, M. Sohail, M. Hasnat, M.M.F.A. Baig, A.U. Ihsan, M. Shumzaid,
882 M.U. Kakar, T. Mehmood Khan, M.D. Akabar, M.I. Hussain, Q.G. Zhou, Chitosan
883 oligosaccharide (COS): An overview, International Journal of Biological
884 Macromolecules. 129 (2019) 827–843. doi:10.1016/j.ijbiomac.2019.01.192.

885 [42] J. Li, D.J. Mooney, Designing hydrogels for controlled drug delivery, Nature
886 Reviews Materials. 1 (2016) 16071 (1–38). doi:10.1038/natrevmats.2016.71.

887 [43] Y. Hong, H. Song, Y. Gong, Z. Mao, C. Gao, J. Shen, Covalently crosslinked chitosan
888 hydrogel: Properties of in vitro degradation and chondrocyte encapsulation, Acta
889 Biomaterialia. 3 (2007) 23–31. doi:10.1016/j.actbio.2006.06.007.

890 [44] S. Düwel, C. Hundshammer, M. Gersch, B. Feuerecker, K. Steiger, A. Buck, A.
891 Walch, A. Haase, S.J. Glaser, M. Schwaiger, F. Schilling, Imaging of pH in vivo using
892 hyperpolarized 13C-labelled zymonic acid, Nature Communications. 8 (2017)
893 15126. doi:10.1038/ncomms15126.

894 [45] S. Dreve, I. Kacso, A. Popa, O. Raita, F. Dragan, A. Bende, G. Borodi, I. Bratu,
895 Structural investigation of chitosan-based microspheres with some anti-

inflammatory drugs, Journal of Molecular Structure. 997 (2011) 78–86. doi:10.1016/j.molstruc.2011.05.001.

[46] J. Schwaiger, H. Ferling, U. Mallow, H. Wintermayr, R.D. Negele, Toxic effects of the non-steroidal anti-inflammatory drug diclofenac: Part I: histopathological alterations and bioaccumulation in rainbow trout, Aquatic Toxicology. 68 (2004) 141–150. doi:https://doi.org/10.1016/j.aquatox.2004.03.014.

[47] E. Gökbulut, İ. Vural, M. Aşıkoğlu, N. Özdemir, Floating drug delivery system of itraconazole: Formulation, in vitro and in vivo studies, Journal of Drug Delivery Science and Technology. 49 (2019) 491–501. doi:10.1016/j.jddst.2018.12.019.

[48] M. Goud, V. Pandey, Gastroretentive drug delivery system, International Journal of Pharma and Bio Sciences. 6 (2016) 158–165.

[49] R.J. Xavier, D.K. Podolsky, Unravelling the pathogenesis of inflammatory bowel disease, Nature. 448 (2007) 427–434. doi:10.1038/nature06005.

[50] B.S.M. Zadeh, F. Moshtaghi, F. Rahim, A. Akhgari, Preparation and evaluation of sodium diclofenac loaded chitosan controlled release microparticles using factorial design, International Journal of Drug Development and Research. 2 (2010) 468–475.

[51] R.B. Kozakevych, Y.M. Bolbukh, V.A. Tertykh, Controlled Release of Diclofenac Sodium from Silica-Chitosan Composites, World Journal of Nano Science and Engineering. 3 (2013) 69–78. doi:10.4236/wjnse.2013.33010.

[52] L. Xinming, C. Yingde, A.W. Lloyd, S. V. Mikhalovsky, S.R. Sandeman, C.A. Howel, L. Liewen, Polymeric hydrogels for novel contact lens-based ophthalmic drug delivery systems: A review, Contact Lens and Anterior Eye. 31 (2008) 57–64. doi:10.1016/j.clae.2007.09.002.

[53] Y. Zhang, X.T. Zhang, Q. Zhang, B. Wang, T. Zhang, Formulation development and evaluation of gastroretentive floating beads with Brucea javanica oil using ionotropic gelation technology, Chinese Journal of Natural Medicines. 16 (2018) 293–301. doi:10.1016/S1875-5364(18)30059-1.